

Direct observation of the magnetic proximity effect in amorphous exchange-spring magnets by neutron reflectometry

A. J. Qviller,* C. Frommen, and B. C. Hauback

Institute for Energy Technology, P.O. Box 40, NO-2027 Kjeller, Norway

F. Magnus

*Division for Materials Physics, Department of Physics and Astronomy,
Uppsala University, Box 516, SE-751 20 Uppsala, Sweden and
Science Institute, University of Iceland, Dunhaga 3, 107 Reykjavik, Iceland*

B. J. Kirby

Center for Neutron Research, NIST, Gaithersburg, Maryland 20899, USA

B. Hjörvarsson

*Division for Materials Physics, Department of Physics and Astronomy,
Uppsala University, Box 516, SE-751 20 Uppsala, Sweden*

(Dated: March 16, 2022)

In this letter we report a direct observation of a magnetic proximity effect in an amorphous thin film exchange-spring magnet by the use of neutron reflectometry. The exchange-spring magnet is a trilayer consisting of two ferromagnetic layers with high T_c 's separated by a ferromagnetic layer, which is engineered to have a significantly lower T_c than the embedding layers. This enables us to measure magnetization depth profiles at which the low T_c material is in a ferromagnetic or paramagnetic state, while the embedding layers are ferromagnetic. A clear proximity effect is observed 7 K above the intrinsic T_c of the embedded layer, with a range extending 50 Å.

Prominent magnetic proximity effects can be obtained at magnetic interfaces [1]. These are present in a variety of magnetic thin films and heterostructures, often having profound effects on the observed magnetic properties [2, 3]. As an example, proximity effects in non-magnetic spacer layers separating two ferromagnets can give rise to long-range interlayer exchange coupling[4], changes in ordering temperature[5] and/or non-oscillatory alignment of magnetic layers[6, 7]. Since layered magnetic structures are ubiquitous in modern technology, the understanding of magnetic proximity effects is of fundamental importance.

In this work we investigate the proximity effect in a ferromagnet-paramagnet system, more specifically in a trilayer [8] of an amorphous exchange-spring magnet[3]. Amorphous heterostructures are free of step edges and grain boundaries and can therefore consist of well defined and smooth layers[9]. The exchange-spring magnet investigated here consists of three ferromagnetic layers, shown schematically in Fig. 1. The top $\text{Co}_{85}(\text{AlZr})_{15}$ layer (A) has an intrinsic T_c well above room temperature and a small imprinted uniaxial anisotropy obtained as described in Ref. [3, 15]. The middle layer (B), which is magnetically isotropic $\text{Co}_{60}(\text{AlZr})_{40}$, is engineered to have a T_c well below room temperature, and much lower than the two other layers. The bottom layer (C) consists of $\text{Sm}_8\text{Co}_{92}$, which has a T_c well above room temperature. Layer C has a large imprinted anisotropy, which can *e.g.* increase the measured coercivity of the adjacent

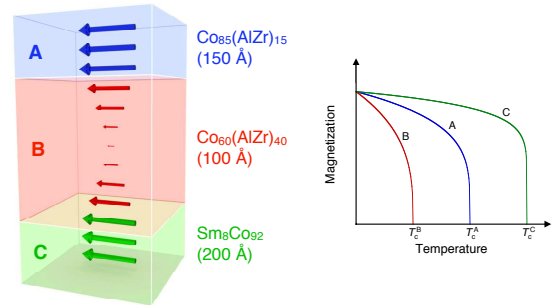


FIG. 1. A schematic representation of the amorphous trilayer and an inferred magnetic proximity effect. The arrows denote the size of the magnetic moments. Layers A and C have a high magnetic ordering temperature whereas layer B has a low ordering temperature as shown on the right. As illustrated in the figure, a pronounced proximity induced magnetization in layer B is expected at temperatures above T_c^B . Figure adapted from reference.[3]

layers. This sample structure has previously been used to indirectly demonstrate that a proximity induced magnetization exists in layer B well above its intrinsic ordering temperature T_c^B [3]. The inferred proximity effect was argued to result in exchange-spring behaviour at temperatures 50% above T_c^B and exchange bias at even higher temperatures. However, no direct information concerning the magnetic state of the center layer was provided.

* Corresponding author; atlejq@gmail.com

Here we provide direct evidence of an induced magnetization in the low- T_c middle layer and we also infer the magnetic profile throughout the layers, using polarized neutron reflectivity measurements [10]. While proximity effects recently have been observed in multilayers [11] with the use of polarized neutron reflectivity, the trilayer sample in this work provides a cleaner and more exact measurement.

The samples were grown by dc magnetron sputtering in a UHV sputtering chamber at an Ar (99.9999 % purity) sputtering gas pressure of 0.27 kPa. First, a 20 Å thick seeding layer of $\text{Al}_{70}\text{Zr}_{30}$ was deposited on a Si(100) substrate (with the native oxide) from an $\text{Al}_{70}\text{Zr}_{30}$ alloy target of purity 99.9%. Subsequently, a 200 Å thick $\text{Sm}_8\text{Co}_{92}$ alloy film was grown by co-sputtering from elemental targets of Co (99.9% purity) and Sm (99.9 % purity), after which a $\text{Co}_{60}(\text{Al}_{70}\text{Zr}_{30})_{40}$ of 100 Å and a $\text{Co}_{85}(\text{Al}_{70}\text{Zr}_{30})_{15}$ layer of 150 Å were grown by co-sputtering from the Co and AlZr targets. Finally, a 30 Å thick capping layer of $\text{Al}_{70}\text{Zr}_{30}$ was grown to protect the underlying magnetic trilayer from oxidation. All films were grown at room temperature. Two permanent magnets provided a magnetic field of approximately 0.1 T parallel to the plane of the films during growth as described in Ref. [15]. This induces a uniaxial in-plane anisotropy in the ferromagnetic layers having an ordering temperature above the growth temperature (A and C). The atomic flux as a function of magnetron power was determined for each target material through X-ray reflectivity measurements of films grown from each of the magnetrons. The power on each magnetron was then set to achieve a given composition while co-sputtering. Rutherford backscattering measurements have previously confirmed that this is a robust method for the materials in question [12, 13]. MOKE measurements were carried out on the samples to confirm the T_c of the middle layer and that the magnetization loops of the trilayers were consistent with previously studied samples. More details on the growth and structural characterization can be found in Refs. 3, 14 and 15.

Polarized neutron reflectivity experiments were carried out at the PBR beamline at NIST at a wavelength of $\lambda = 4.75$ Å using an instrument resolution of $\Delta\lambda/\lambda = 0.01$. Four reflectivities, corresponding to the two non-spin-flip channels (R^{++} and R^{--}) as well as the two spin-flip channels (R^{-+} and R^{+-}), were measured out to $q = 0.2$ Å $^{-1}$ at $T_1 = 300$ K, $T_2 = 110$ K and $T_3 = 10$ K. With $T_c^B = 103 \pm 1$ K [3] (see Figure 1), these temperatures correspond to $T_1 \gg T_c^B$, $T_2 > T_c^B$ and $T_3 < T_c^B$. Samples were measured with an applied external field of $\mu_0 H = 10$ mT along the easy axis of the imprinted anisotropy and the scattering plane perpendicular to this axis. Measurements of the spin-flip reflectivities returned mainly noise, consistent with the presence of a collinear magnetization state [10], which is reasonable in the given measurement configuration. The spin-flip reflectivities were therefore subsequently disregarded in the fitting process.

Data were fitted using the GenX 2.4.7 reflectivity pack-

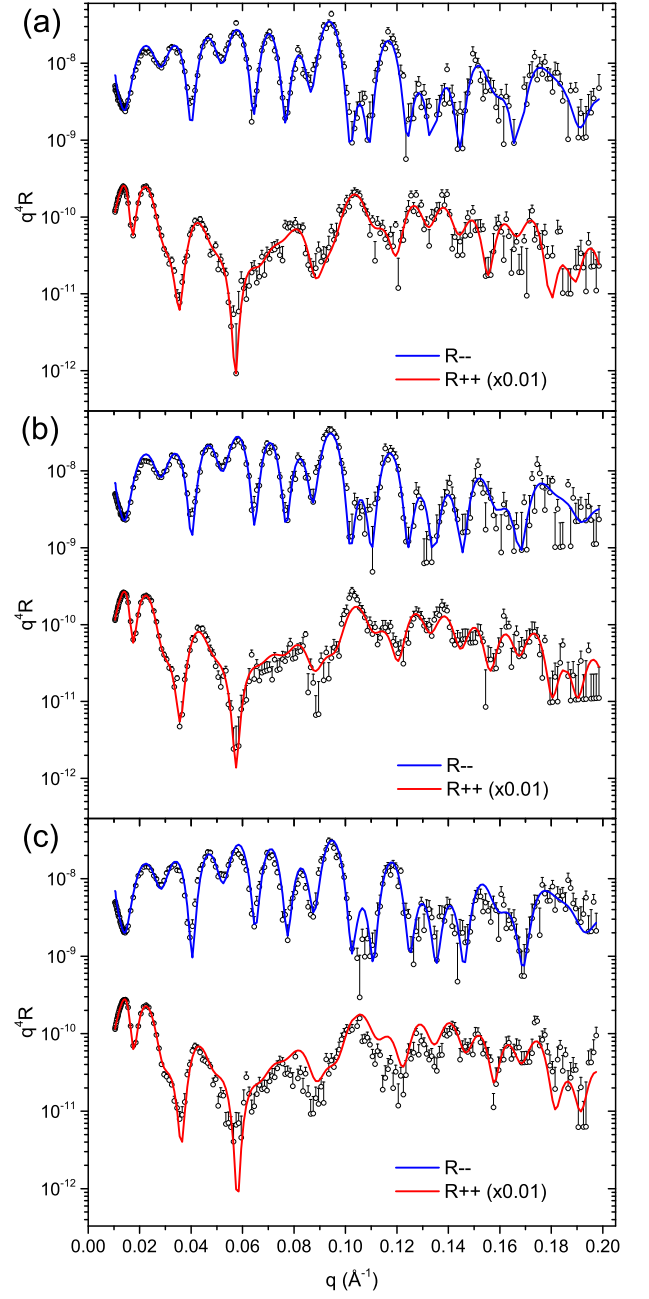


FIG. 2. Non-spin-flip polarized neutron reflectivity scans, R^{--} and R^{++} , measured at $\mu_0 H = 10$ mT and (a) $T = 300$ K, (b) $T = 110$ K and (c) $T = 10$ K. Fits are shown as solid lines in red and blue. Error bars correspond to ± 1 standard deviation and are shown only on the upper side for clarity.

age with the new MagRefl module [16], using the logarithm of the reflectivity as the figure of merit. The sample model consists of a partially oxidised capping layer (oxide consisting of a 70/30 mixture of $\text{Al}_2\text{O}_3/\text{ZrO}_2$ and an $\text{Al}_{70}\text{Zr}_{30}$ layer), a magnetic $\text{Co}_{85}(\text{AlZr})_{15}$ layer, a magnetic $\text{Co}_{60}(\text{AlZr})_{40}$ interlayer, a magnetic $\text{Sm}_8\text{Co}_{92}$ layer and a seeding layer of $\text{Al}_{70}\text{Zr}_{30}$ on a thin SiO_2 layer on a Si substrate (see Figure 3). Most structural parameters were determined by fitting the results obtained at $T = 300$ K and $\mu_0 H = 10$ mT. Reflectivity measurements

cannot be used alone to determine the chemical composition of layers consisting of more than two elements, but the validation of the sample preparation procedure stated above justifies fixing the stoichiometry of the layers to the intended values and only allowing their densities to vary during the fitting at $T = 300$ K and $\mu_0 H = 10$ mT. In the simulations, the low- T_c layer was defined by 10 slices and the magnetic moments of these layers were fitted to a sum of two power laws with the same exponent, one corresponding to a decaying magnetization from each interface, induced by the neighbouring ferromagnetic layers as illustrated in Fig. 1. A power law decay of the magnetization was chosen as it is the functional form of the long-range exchange interaction, as *e.g.* described in Refs. 3 and 17. The resulting step-wise magnetic profile was smoothed by allowing a small, linked chemical roughness (7 \AA RMS) for each slice. Only the magnetization of the three ferromagnetic layers and their profiles were allowed to vary when fitting the data obtained at $T = 110$ K and $T = 10$ K. Additionally, changes in thickness were needed to account for the thermal expansion in the layers, which was determined to be $4.1 \times 10^{-5} \text{ K}^{-1}$, or 1.2 % when heating the sample from $T = 10$ K to $T = 300$ K. Notice that the determined thermal expansion only holds for the combined film and substrate, where the substrate provides elastic boundaries defining the changes in the lateral direction with temperature, due to clamping effects. The resulting polarized neutron reflectivity results (scaled in q) and corresponding fits are shown in Fig. 2 (a), (b) and (c).

The determined chemical and magnetic SLD profiles at $\mu_0 H = 10$ mT and $T = 300$ K are shown in Fig. 3 (a), as functions of the distance from the substrate z . The chemical SLD profile yields interface roughnesses equal to or less than 8 \AA RMS. Inferred magnetic SLD profiles are shown in Fig. 3 (b). When $T = 300$ K and $\mu_0 H = 10$ mT (green line), no magnetization is observed in the middle of layer B. Furthermore, the magnetization at the interfaces decays sharply, consistent with relatively short ranged magnetic proximity effects. At the lowest temperature, $T = 10$ K (black line), the middle layer is magnetized, as expected since this is well below the ordering temperature of layer B. Significant magnetization is seen throughout the middle layer at $T = 110$ K (red line) which is well above the ordering temperature of the layer (7 K above T_c^B). This observation can be viewed as a manifestation of a long range magnetic proximity effect, where a magnetization is induced in layer B well above its intrinsic ordering temperature due to the proximity to the high- T_c layers A and C. Error bars for the magnetization in the middle of layer B as measured by reflectometry were determined by inspection of how much it can change before the fits become visually worse. This was 7% for both the $T = 10$ K data and the $T = 110$ K data. For technical reasons, the latter error bar in absolute terms was also used for the interlayer magnetization at $T = 300$ K.

As there is a significant magnetization in the center of the 100 \AA thick layer B, it can be deduced that the range

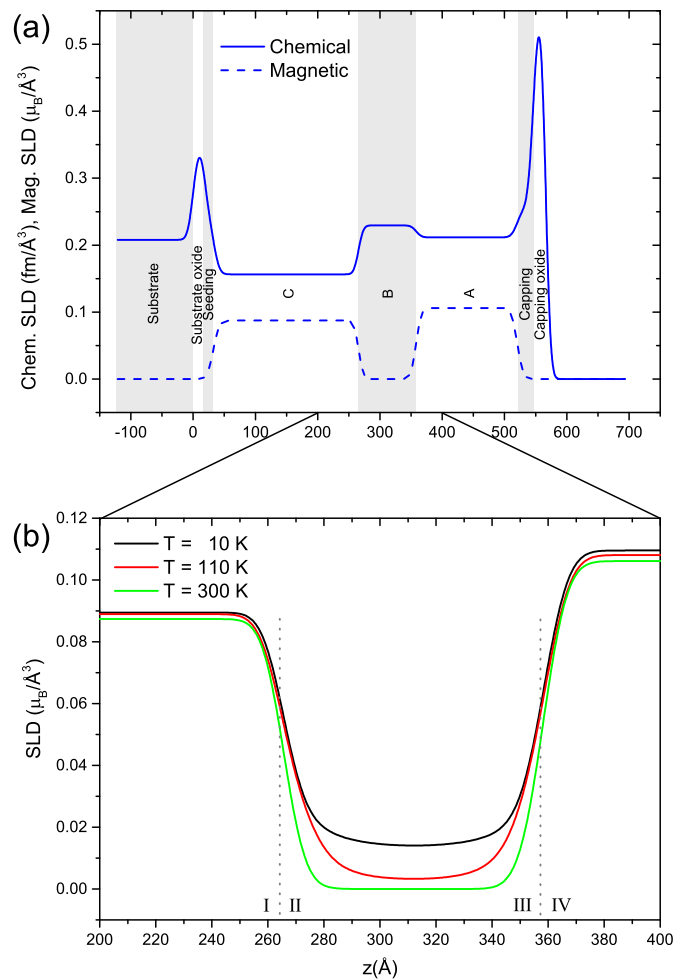


FIG. 3. (a) Chemical and magnetic SLD profiles at $\mu_0 H = 10$ mT and $T = 300$ K for the entire exchange-spring magnet heterostructure. The capping layer, layers A, B, C, the seeding layer and the substrate are indicated. Oxide layers on the capping layer and substrate are also marked. (b) Magnetization profiles of the low- T_c $\text{Co}_{60}(\text{AlZr})_{40}$ middle layer and its interfaces at $\mu_0 H = 10$ mT, $T = 10, 110$ and 300 K. Error bars (not shown) of the magnetization in the center of this layer are 7% for all temperatures. The magnetization profiles at $T = 10$ K and 110 K have been offset to correct for the measured thermal expansion.

of the proximity effect is at least 50 \AA at $T = 110$ K. This is consistent with the interpretation of previous experimental results and requires an explanation in terms of long-range effective exchange interactions [3]. Monte Carlo simulations have shown that an extended region of induced magnetization can only be expected in layer B, if interactions beyond nearest neighbour are accounted for. Furthermore, atomic correlations in terms of regions of higher Co-density can further amplify the proximity effect, as discussed in Ref. 3. Interdiffusion can be ruled out as the cause of the induced magnetization in layer B due to the very different length scales of its range and the magnitude of the interface roughnesses, and that the measured interdiffusion can not depend on the measure-

TABLE I. Absolute value of the half-width half maxima of the derivative of the magnetic SLD profiles.

Temperature (K)	I (Å)	II (Å)	III (Å)	IV (Å)
10 \pm 1	7.3	8.7	9.1	8.3
110 \pm 1	8.3	12	12	8.6
300 \pm 1	7.4	7.3	9.1	7.9

ment temperature.

To investigate the spatial dependence of the magnetization with temperature, the absolute value of the derivative of the magnetic SLD profiles in Fig. 3 (b) was calculated. Four half-widths at half maxima were extracted, describing the spatial change in magnetization at the interfaces of the layers. The results are provided in Table I, the annotations of the interfaces I-IV are defined in Fig. 3 (b). The widths I and IV describe the change in the magnetization of the outer boundaries of layers A and C. These are found to be independent of temperature, as expected. The changes in width II (III) describes the changes in the magnetization profile of the interface of A (C) and B. At $T = 10$ K, all the layers are close to fully magnetic and the deduced magnetization profile resembles therefore primarily the distribution of the elements in the sample. At $T = 300$ K, the magnetization and susceptibility of layer B is negligible and the width is therefore dominated by the interface effects of layers A and C, at both the interfaces. Thus the width of the magnetic profile obtained at these temperatures are expected to be similar, which is consistent with the obtained results. We can now compare these with the results obtained at $T = 110$ K. The width of the magnetic profile in region II and III is clearly larger at this temperature, as seen

in Table I. In order to underpin the above analysis, a normal probability plot of the values in Table I was done (not shown). It revealed that the widths in region II and III at $T = 110$ K are outliers at 2.0σ , while the rest of the observations are approximately normally distributed around a sample mean of 8.8 Å . The above discussion reflects the expected changes in the magnetic susceptibility, which is largest at T_c . Monte Carlo simulations involving beyond nearest neighbour magnetic interactions show that not only is the peak in the magnetic susceptibility shifted to higher temperature, but it is also significantly broadened, due to proximity effects. [3] This is well reflected in the present results, however, the magnetization of the centre of the layer is not captured by these simulations. An analogous effect arising from changes in the effective coupling due to changes in the local concentration has previously been described for random alloys [18]. The spatially dependent changes in the concentration of the elements in a magnetic alloy will give rise to changes in the effective magnetic coupling. The magnetization will consequently decline in a non-uniform way, giving rise to partially coupled ferromagnetic regions. This, in combination with long range interaction can therefore serve as a basis of the understanding of the observed proximity effects, well above its intrinsic ordering temperature.

The Research Council of Norway is acknowledged for financial support through the SYNKNØYT program, project 218418. This work was also funded by the Swedish Research Council (VR) and the Knut and Alice Wallenberg Foundation (KAW). FM acknowledges funding from the Icelandic Research Fund grant no. 174271-051. AJQ would like to express his gratitude to Bengt Lindgren for his skillful assistance with modelling in GenX.

-
- [1] R. M. White and D. J. Friedman, "Theory of the magnetic proximity effect," *J. Magn. Magn. Mater.* **49**, 117–123 (1985).
 - [2] P. K. Manna and S. M. Yusuf, "Two interface effects: Exchange bias and magnetic proximity," *Phys. Rep.* **535**, 61–99 (2014).
 - [3] F. Magnus, M. E. Brooks-Bartlett, R. Moubah, R. A. Procter, G. Andersson, T. Hase, S. T. Banks, and B. Hjörvarsson, "Long-range magnetic interactions and proximity effects in an amorphous exchange-spring magnet," *Nat. Commun.* **7**, ncomms11931 (2016).
 - [4] N. J. Gökemeijer, T. Ambrose, and C. L. Chien, "Long-range exchange bias across a spacer layer," *Physical Review Letters* **79**, 4270–4273 (1997).
 - [5] U. Bovensiepen, F. Wilhelm, P. Srivastava, P. Pouloupoulos, M. Farle, A. Ney, and K. Baberschke, "Two Susceptibility Maxima and Element Specific Magnetizations in Indirectly Coupled Ferromagnetic Layers," *Phys. Rev. Lett.* **81**, 2368–2371 (1998).
 - [6] W. L. Lim, N. Ebrahim-Zadeh, J. C. Owens, H. G. E. Hentschel, and S. Urazhdin, "Temperature-dependent proximity magnetism in Pt," *Appl. Phys. Lett.* **102**, 162404 (2013).
 - [7] M. Gottwald, J. J. Kan, K. Lee, S. H. Kang, and E. E. Fullerton, "Paramagnetic $\text{Fe}_x\text{Ta}_{1-x}$ alloys for engineering of perpendicularly magnetized tunnel junctions," *APL Mater.* **1**, 022102 (2013).
 - [8] E. E. Fullerton, J. S. Jiang, M. Grimsditch, C. H. Sowers, and S. D. Bader, "Exchange-spring behavior in epitaxial hard/soft magnetic bilayers," *Phys. Rev. B* **58**, 12193–12200 (1998).
 - [9] C.-M. Choi, J.-O. Song, and S.-R. Lee, "Thermal stability of magnetic tunnel junctions with new amorphous ZrAl-alloy films as the under and capping layers," *IEEE T. Magn.* **41**, 2667–2669 (2005).
 - [10] H. Zabel, "X-ray and neutron reflectivity analysis of thin films and superlattices," *Applied Physics A Solids and Surfaces* **58**, 159–168 (1994).
 - [11] K. A. Thórarinsdóttir, H. Palonen, G. K. Palsson, B. Hjörvarsson, and F. Magnus, "Giant magnetic proximity effect in amorphous layered magnets," *Phys. Rev. Materials* **3**, 054409 (2019).
 - [12] A. Liebig, P. T. Korelis, H. Lidbaum, G. Andersson, K. Leifer, and B. Hjörvarsson, "Morphology of amorphous $\text{Fe}_{91}\text{Zr}_9/\text{Al}_2\text{O}_3$ multilayers: Dewetting and crystallization," *Phys. Rev. B* **75**, 214202 (2007).

- [13] A. Frisk, F. Magnus, S. George, U. B. Arnalds, and G. Andersson, "Tailoring anisotropy and domain structure in amorphous TbCo thin films through combinatorial methods," *J. Phys. D: Appl. Phys.* **49**, 035005 (2016).
- [14] F. Magnus, R. Moubah, A. H. Roos, A. Kruk, V. Kapaklis, T. Hase, B. Hjörvarsson, and G. Andersson, "Tunable giant magnetic anisotropy in amorphous SmCo thin films," *Appl. Phys. Lett.* **102**, 162402 (2013).
- [15] H. Raanaei, H. Nguyen, G. Andersson, H. Lidbaum, P. Korelis, K. Leifer, and B. Hjörvarsson, "Imprinting layer specific magnetic anisotropies in amorphous multilayers," *J. Appl. Phys.* **106**, 023918 (2007).
- [16] M. Björck and G. Andersson, "GenX: an extensible X-ray reflectivity refinement program utilizing differential evolution," *J. Appl. Crystallogr.* **40**, 1174–1178 (2007).
- [17] M. E. Fisher, S. Ma, and B. G. Nickel, "Critical Exponents for Long-Range Interactions," *Phys. Rev. Lett.* **29**, 917–920 (1972).
- [18] R. Gemma, M. to Baben, A. Pundt, V. Kapaklis, and B. Hjörvarsson, "The impact of nanoscale compositional variation on the properties of amorphous alloys," *arXiv* **1811:03354** (2018).